Journal of Materials Chemistry

www.rsc.org/materials

Volume 22 | Number 44 | 28 November 2012 | Pages 23279–23688

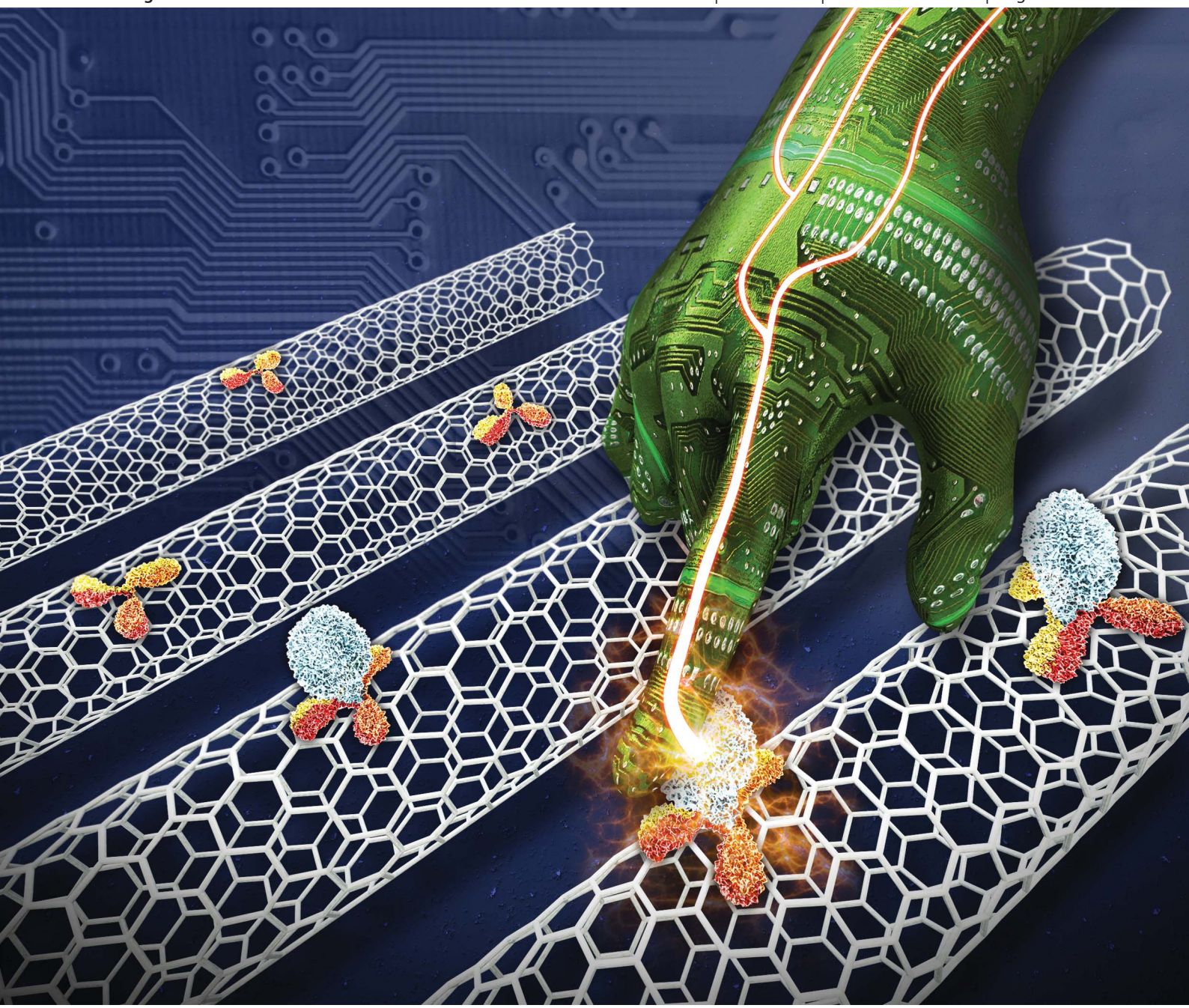

ISSN 0959-9428

RSC Publishing

PAPER

Dae Sung Yoon, Taeyun Kwon *et al.*

Aptamer-functionalized nano-pattern based on carbon nanotube for sensitive, selective protein detection

0959-9428(2012)22:44;1-9

Journal of Materials Chemistry

Dynamic Article Links

Cite this: J. Mater. Chem., 2012, 22, 23348

www.rsc.org/materials

PAPER

Aptamer-functionalized nano-pattern based on carbon nanotube for sensitive, selective protein detection†

Kihwan Nam,‡[ab] Kilho Eom,‡[ab] Jaemoon Yang,[c] Jinsung Park,[d] Gyudo Lee,[ab] Kuewhan Jang,[d] Hyungbeen Lee,[b] Sang Woo Lee,[b] Dae Sung Yoon,*[ab] Chang Young Lee[e] and Taeyun Kwon*[ab]

Received 8th June 2012, Accepted 29th August 2012
DOI: 10.1039/c2jm33688j

We have developed a horizontally aligned carbon nanotube sensor that enables not only the specific detection of biomolecules with ultra-sensitivity, but also the quantitative characterization of binding affinity between biomolecules and/or interaction between a carbon nanotube and a biomolecule, for future applications in early diagnostics. In particular, we have fabricated horizontally aligned carbon nanotubes, which were functionalized with specific aptamers that are able to specifically bind to biomolecules (*i.e.* thrombin). Our detection system is based on scanning probe microscopy (SPM) imaging for horizontally aligned aptamer-conjugated carbon nanotubes (ACNTs) that specifically react with target biomolecules at an ultra-low concentration. It is shown that the binding affinity between thrombin molecule and ACNT can be quantitatively characterized using SPM imaging. It is also found that the smart carbon nanotube sensor coupled with SPM imaging permits us to achieve the high detection sensitivity even up to ~1 pM, which is much higher than that of other bioassay methods. Moreover, we have shown that our method enables a quantitative study on small molecule-mediated inhibition of specific biomolecular interactions. In addition, we have shown that our ACNT-based system allows for the quantitative study of the effect of chemical environment (*e.g.* pH and ion concentration) on the binding affinity. Our study sheds light on carbon nanotube sensor coupled with SPM imaging, which opens a new avenue to early diagnostics and drug screening with high sensitivity.

Introduction

The specific, sensitive recognition of target biomolecules inherent in patients is an *a priori* requisite for the precise, early diagnosis of various diseases such as cancer and cerebral/cardiovascular diseases. For such a sensitive detection, aptamers based on nucleic acids have been recently highlighted as probes that can specifically sense and detect target biomolecules (*i.e.* proteins and nucleic acids) due to their high binding affinity, reusability, and selectivity.[1–7] In particular, aptamers can be chemically modified, easily denatured, and refolded in a repetitive manner without loss of activity, indicating the potential of aptamers for the development of efficient sensing elements.[8–12] Furthermore, aptamers are in the form of molecular chain rather than a complicated molecular structure as is a protein, which implies that aptamers enable the formation of a dense, mono-layered sensing element with a high binding affinity to target biomolecules.[8] As a consequence, surface engineering using aptamers as capturing probes has been recently taken into account to achieve high recognition sensitivity.

Furthermore, for sensitive detection, the method to sense the binding events between probes and target molecules has been established based on nanotechnology and this leads to sensitive *in vitro* detection. Recently, scanning probe microscopy (SPM) has been considered as a sensing toolkit to identify the specific, sensitive target biomolecules due to the high spatial resolution (even up to nanometer scale).[13,14] The fundamental principle for SPM-based detection is the direct transduction of the interaction between the SPM tip and the biological sample into the mechanical response (*e.g.* frequency change or deflection change) of the SPM cantilever.[15] For instance, tapping mode atomic force microscopy (tmAFM)[16,17] and Kelvin probe force microscopy (KPFM)[18–21] have enabled the sensitive detection of biomolecules such as DNA, RNA, and proteins. In addition, SPM does not require the cumbersome processes in sampling such as labeling of

[a]*Institute for Molecular Sciences, Seoul, 120-752, Republic of Korea*
[b]*Department of Biomedical Engineering, Yonsei University, Wonju, 220-710, Republic of Korea. E-mail: tkwon@yonsei.ac.kr; dsyoon@yonsei.ac.kr*
[c]*Department of Radiology, College of Medicine, Yonsei University, Seoul, 120-752, Republic of Korea*
[d]*Department of Mechanical Engineering, Korea University, Seoul, 136-701, Republic of Korea*
[e]*School of Nano-Bioscience and Chemical Engineering, Ulsan National Institute of Science and Technology (UNIST), Ulsan, 689-798, Republic of Korea*

† Electronic supplementary information (ESI) available. See DOI: 10.1039/c2jm33688j

‡ These authors made equal contribution to this work.

target molecules using fluorescence dyes; this implies that the fabrication of the sensing substrate is a cost-effective and straightforward.

In this study, we have developed a novel, *in vitro* diagnostic system based on a combination of aligned aptamer-conjugated carbon nanotubes (ACNTs) and SPM for not only the ultra-sensitive biomolecular detection but also quantitative studies on binding affinities between biomolecules (see Fig. 1). It should be noted that a quantitative insight into the binding affinity between the target biomolecule and the probe biomolecule (used for the functionalization of the sensing surface) is essential for the effective design of sensors that enable the sensitive detection. In this work, the ACNT was constructed through the immobilization of aptamers onto a horizontally aligned carbon nanotube (CNT) on the silicon substrate (without lithography). The high detection sensitivity of ACNT is attributed to the formation of dense aptamer monolayer as well as the minimal sensing area due to the small diameter of the CNT (~4 nm). For validation of ACNT as the ultrasensitive diagnostic toolkit, a thrombin was considered as a representative target biomolecule in order to quantify concentration-dependent binding affinities between ACNT and target biomolecules using SPM (tmAFM/KPFM) imaging techniques. It is shown that horizontally aligned ACNTs coupled with SPM imaging allow for quantitative study of the binding affinity between the biomolecule and the ACNT sensor, which is an *a priori* requisite for the development of a sensing toolkit enabling label-free protein detection with high sensitivity. It is also shown that our ACNT is able to characterize the binding affinity between ACNT and thrombin molecule even in ultra-low concentrations (such as 1 pM). Moreover, we have shown that aligned ACNTs are appropriate for the quantitative understanding of small molecule-mediated inhibition of thrombin–DNA interactions, and that ACNT is capable of characterizing the effect of chemical environment (such as pH and ion concentration) on the binding affinity. Our study suggests that ACNTs may be useful as a sensing toolkit in future applications for sensitive drug screening in a label-free manner.

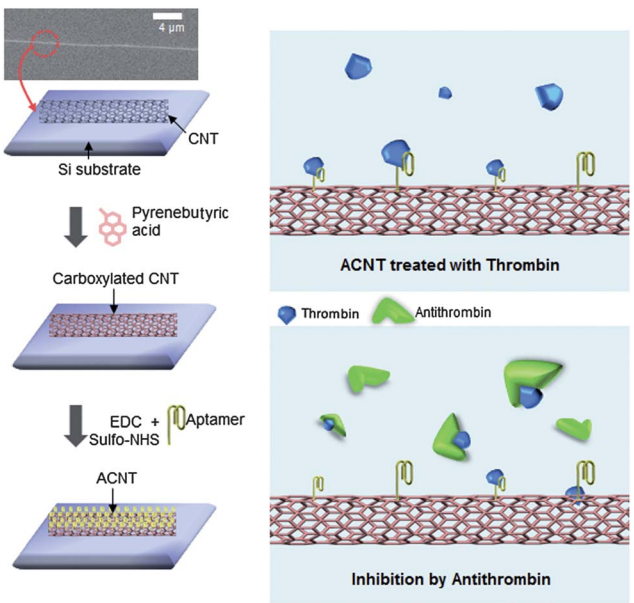

Fig. 1 Schematic illustration of the development of the aptamer-modified carbon nanotube (ACNT) and ACNT-based biomolecular detection *via* scanning probe microscopy. A carbon nanotube (CNT) as shown in an inset (scanning electron microscopy image) was horizontally grown *via* chemical vapor deposition (CVD) on the Si-substrate, and it can act as a nanoscale line pattern for fabrication of ACNT. When thrombin molecules only were injected, the ACNT is selectively able to capture the thrombin molecules. When the ACNT was exposed to both thrombin molecules and antithrombin molecules at the same time, antithrombin molecules are likely to hamper the binding between the thrombin molecules and the ACNT.

Experiment

Fabrication of ACNT

For the nanoscale patterning on the substrate, we have chemically fabricated the CNT in such a way that CNTs were chemically grown from a catalyst deposited on the substrate through a chemical vapor deposition (CVD) method (see ESI, Fig. S1†). Here, iron as a catalyst for CNT growth was deposited onto a silicon wafer *via* a thermal evaporator with thickness of 0.5 Å. Then the silicon substrate (where iron was deposited) with its dimension of 1 cm × 1 cm was put into the quartz tube, which resides inside another quartz tube in a furnace. After locating the sample inside the quartz tube in the furnace, the catalyst-evaporated silicon wafer was annealed at a temperature of ~500 °C and then cooled down to room temperature in air. After annealing, CNT growth was conducted by injecting H_2 and CH_4 gases at a temperature of ~1000 °C. After CNT growth, the injection of gases such as H_2 and CH_4 was halted, and the furnace is cooled down by injection of N_2 gas.[22,23]

The average diameter of fabricated CNTs is ~4.4 nm. As shown in the inset of Fig. 1, which shows the scanning electron microscope (SEM) images, CNTs were grown straight on the substrate, which indicates that CNTs can serve the nanoscale patterned lines. For the development of ACNT, the surface of a CNT was first functionalized using 1-pyrenebutyric acid (1 mg, 97%, Sigma-Aldrich, USA) in 10 mL *N*,*N*-dimethylformamide (99%, Sigma-Aldrich, USA), which results in the carboxyl group being formed on the surface of CNT due to the π–π stacking interactions. In general, CNTs could be functionalized with carboxyl groups based on two different methods; (i) oxidation of the CNT for covalent bonding and (ii) non-covalent bonding onto the CNT sidewall.[24–26] However, the oxidation method causes damage to the CNT surface; this defect in CNT sidewall can lead to a critical problem such as the clustering of analytes due to an acetone around the carboxylated CNT *via* intermolecular binding.[27] We have, therefore, functionalized the CNT through carboxylation with a π–π stacking interaction that has a strong bond between the pyrene-modified probe molecules and the CNT.[28] After the reaction for 24 hours at room temperature, the carboxylated nanotubes were purified by deionized water (Millipore, USA). For conjugation of the aptamer onto the nanotube, we prepared a Tris–EDTA (TE) buffer solution (1 mL, pH 8.0) that contains 1-ethyl-3-[3-dimethylamino-propyl] carbodiimide hydrochloride (1 mg, Thermo Scientific Pierce, USA) and *N*-hydroxysulfosuccinimide (1 mg, Thermo Scientific Pierce, USA). This solution activates the carboxyl group which is

able to form an amide bond with the amine group of a biomolecule as a receptor molecule. Subsequently, the nanotubes were reacted with such a prepared solution for 30 minutes and then rinsed with deionized water. For the functionalization of carboxylated nanotubes with aptamer, we dropped the TE buffer solution in which the aptamer was dissolved. Here, we used the aptamer whose sequence is given as 5′-amine-TTT TTT GGT TGG TGT GGT TGG-3′ (COSMO, Korea). In addition, for the preparation of the solution containing the aptamer, the aptamer was diluted in TE buffer solution (pH 8.0) such that the dissolved solution (for an amount of 100 μL) contains the aptamers at a concentration of 10 μM. Finally, after incubation for 2 hours at room temperature, the nanotubes functionalized with DNA aptamers were rinsed using deionized water.

Fluorescence images of ACNT

We have performed an imaging of ACNT using fluorescence microscopy (IX71, Olympus, Japan) in order to verify the formation of aptamers on the CNT surface. Here, we used the complementary DNA (cDNA) whose sequence is given as 5′-FITC-CCC ACC ACA CCA ACC AAA AAA-3′ (COSMO, Korea). For the preparation of ACNT bound to cDNA, we have incubated the ACNT in the buffer solution (pH 8.0; 100 μL), which contains cDNA (at a concentration of 10 μM), for 2 hours. Then, we have rinsed the ACNT in order to eliminate physisorption. For imaging the thrombin molecules bound to ACNT, we have used thrombin molecules that are labeled with Cy3 (abcam, USA). For imaging the binding between thrombin and ACNT, we have incubated the ACNT in a buffer solution (pH 7.4; 100 μL), which contains thrombin molecules tagged with Cy3 (at a concentration of 10 μM), for 2 hours. To eliminate physisorption, we have rinsed the ACNT with deionized water.

Bioassay

We consider thrombin (50–300 NIH units mg^{-1} protein, Sigma-Aldrich, USA) as a target protein in the experiment. Thrombin molecules were diluted in PBS buffer solution (pH 7.4) such that thrombin concentrations range from 1 pM to 1 nM. 100 μL of the thrombin dissolved solution was dropped onto the ACNT patterned substrate and maintained for 2 hours. Subsequently, the ACNT patterned substrate was rinsed with deionized water and dried in vacuum for 12 hours, and then imaged by scanning probe microscopy (SPM) techniques such as tmAFM and KPFM, which will be described below. For the inhibition assay, we have utilized antithrombin III (≥95%, Sigma-Aldrich, USA) as an inhibitor molecule that can prevent the thrombin–aptamer binding. Antithrombin III was diluted in PBS buffer solution (pH 7.4) such that antithrombin concentration is in the range of 1 pM to 1 nM. We dropped the solution (100 μL), which contains both thrombin (at a concentration of 100 pM) and antithrombin (at various concentrations ranging from 10 pM to 10 nM), onto the ACNT patterned substrate. Then, the ACNT to which the solution was dropped was maintained for 2 hours in order to guarantee sufficient reaction between the aptamer (functionalized on CNT), thrombin, and antithrombin. It is noted that the incubation time (*i.e.* 2 h in our assay) can be reduced because most of the biomolecular interaction occurs within 30 min.[29] Finally, the ACNT patterned substrate was rinsed with deionized water and kept in vacuum for 12 hours in order to remove the physisorbed molecules on the ACNT. Here, the rinsing time can be also reduced as elucidated in ref. 19.

Scanning probe microscopy (SPM)-based imaging

In the experiment, all images of ACNT after bioassay were acquired using a lift mode that enables not only tmAFM imaging but also KPFM imaging. In other words, both tmAFM and KPFM images can be simultaneously obtained from the lift-mode at the scanned location. The SPM-based measurement was performed using PicoForce (Veeco Inc., Santa Barbara, CA, USA) with Nanocontroller V (Veeco Inc.) under an ambient condition at room temperature. To obtain images, we have utilized a SCM-PIT tip (Veeco Inc.), which is coated with Pt/Ir (front layer) and Cr (bottom layer), as a scanning probe. Here, the SCM-PIT tip has a normal resonant frequency of 75 kHz and a tip radius of ~20 nm. The tmAFM/KPFM images were acquired based on scanning speed of 1 μm s^{-1}, which is a suitable speed to guarantee high quality images. We obtained tmAFM/KPFM images with a scan size of 1 μm × 1 μm, which is a proper scan size to image a couple of ACNTs on the substrate. For KPFM imaging, we have to set up the parameters for KPFM imaging before implementation of KPFM imaging. In order to tune the feedback parameters (*e.g.* phase, proportional and integral gains), we have checked the surface potential profile of a bare CNT, which was grown horizontally on the substrate, and then the feedback parameters were adjusted. KPFM images were obtained such that KPFM tip is distant from the substrate by 5 nm, and a voltage of 1 V alternating current (AC) was applied to the tip. Here, the sample was grounded using a carbon tape and silver paste (Dotite, Japan). This ground system enables us to reduce both the error signal and charge-up phenomena. For accurate imaging, we have used the same cantilever tip during the imaging of ACNTs in different states such as thrombin-bound state and/or antithrombin-inhibited state. All SPM images were generated from Nanoscope software V7.2.

Results

Fabrication of aligned aptamer-modified carbon nanotubes

Despite its ability to image and sense proteins, SPM itself is not suitable for label-free protein detection for future diagnostic applications. In particular, it is required to prepare a sensing surface that is able to selectively and specifically capture target protein molecules. Moreover, for high detection sensitivity, it is desirable to introduce a patterned surface which permits target proteins to be bound to a limited region of a sensing surface. For instance, Yang *et. al.*[30] have introduced the nanoparticle-modified surface in order to increase the binding affinity between the target cells (*e.g.* cancer cells) and the sensing surface. A recent study[31] has reported a nanopillar-modified sensing surface that allows for the sensitive detection of circulating tumor cells. A previous study[16,32] suggested a DNA-patterned surface using nanoshaving and nanografting methods for highly sensitive DNA detection. It should be noted that conventional surface patterning is not a cost-effective fabrication method, although it allows for the enhancement of detection sensitivity.

Here, we are aimed at developing a cost-effective fabrication method for the preparation of a sensing surface without requiring any expensive patterning processes. Fig. 1 provides a schematic illustration of the preparation of a sensing surface based on horizontally aligned CNTs. In particular, we have prepared a surface, on which individual CNTs are horizontally aligned, in order for the sensing surface to capture target protein molecules with a high detection sensitivity due to the protein binding onto a limited area of the sensing surface (*i.e.* the surface area of the horizontally grown CNT). Since the surface area of a CNT on a substrate occupies a limited area of the substrate, a small number of target molecules could be bound to a CNT-modified sensing surface; this surface can detect target molecules even in low concentrations due to the specific binding between the target molecules and CNTs on a substrate. Moreover, for a label-free detection based on SPM imaging of a sensing surface, it is required that the CNT has to be continuously and grown straight on a substrate since CNT has to exhibit a uniform diameter along its longitudinal direction. If the diameter of the CNT is not uniform during the chemical growth, then a non-uniformly grown CNT on a substrate is not suitable for SPM imaging-based detection because SPM imaging encounters difficulties in identifying target protein molecules bound to a non-uniformly grown CNT. The inset of Fig. 1 shows that the diameter of the single-walled CNT is 4.4 ± 1.5 nm (with roughness of <1 nm) along the longitudinal direction of CNT, which indicates the continuous growth of the CNT on the substrate. The measured diameter of a single-walled CNT is consistent with a previous study[33] reporting that the diameter of a single-walled CNT is in a range of 3 nm to 5 nm. Moreover, in order for the CNT-modified surface to have a binding affinity to specific target molecules with high selectivity, we have chemically functionalized the CNTs using DNA aptamers. To validate the high selectivity of the CNT-based surface, we have considered the fluorescence image of such a surface that was immersed in a solution containing target molecules (at a concentration of 10 μM) in order to induce the reaction between the target molecules and the sensing surface. Fig. 2 shows that target molecules are only bound to ACNTs patterned as a straight line on a substrate (see also Fig. S2 showing the fluorescence image of a negative control experiment in the ESI‡), which indicates that the target molecules can be selectively bound to the ACNT. In particular, Fig. 2(a) shows the fluorescent image of complimentary DNA molecules (tagged with FITC) that are specifically bound to ACNT, while Fig. 2(b) depicts the fluorescent image of thrombin molecules (tagged with Cy3) that are specifically captured by the ACNT. Fig. 2(b) clearly verifies the attachment of protein molecules (*i.e.* thrombin molecules) onto the ACNT. It clearly elucidates that a CNT-based sensing surface may enable the highly sensitive detection of target molecules without requiring expensive lithography (to introduce the pattern on a substrate).

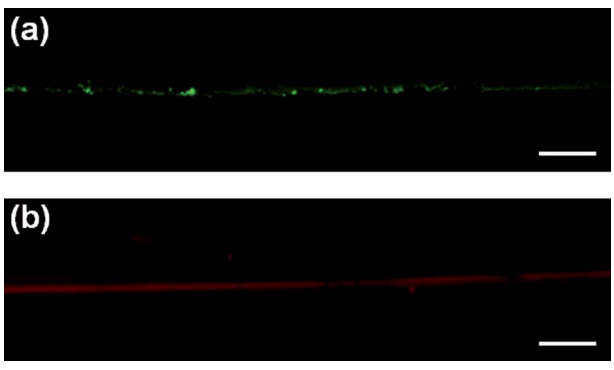

Fig. 2 Fluorescence images (a) ACNT reacted with complementary DNA tagged with FITC label. Scale bar is 40 μm. (b) ACNT reacted with thrombin labeled with Cy3. Scale bar is 25 μm.

Protein bioassay

Fig. 3(a)–(c) depicts the tmAFM/KPFM images and their corresponding height and surface potential profiles (see Fig. 3(e)–(g)) for a CNT, ACNT and ACNT treated with thrombin (1 nM). The CNT was grown in a straight line-pattern on a silicon (Si) substrate such that the average height of the CNT obtained by tmAFM image was 4.4 ± 1.5 nm. The surface potential of the CNT was relatively positive (~42.9 mV) in comparison with that of the Si substrate due to the different work functions between the CNT (~4.9 eV) and the slightly oxidized Si substrate (5.12 eV).[34] The conjugation of aptamers (M_W: 196.2 Da) to a CNT increases the height profile by an amount of ~2 nm with little roughness (<1 nm), indicating that the aptamers were uniformly immobilized as a dense monolayer onto the CNT. Due to the negative charge of the nucleic acid backbone of aptamers, the surface potential of the ACNT was negative with a value of −142.5 mV. For an evaluation of the robustness of the ACNT as a diagnostic tool, we have considered tmAFM/KPFM imaging and their corresponding profiles for the ACNT that was reacted with thrombin at a concentration of 1 nM. Fig. 3(a)–(c) shows that tmAFM/KPFM is able to identify thrombin molecules bound to the ACNT. Specifically, the average height of the ACNT treated with thrombin is about twice as large as that of an ACNT, while the ACNT treated with thrombin exhibits a relatively negative charge (−263.8 mV) compared with that of an ACNT. The increased height due to the thrombin binding onto the ACNT is ascribed to the molecular size and complex structure of thrombin,[35] while the decrease in the surface potential is attributed to the isoelectric point (7.0 for thrombin) that is lower than the pH of buffer solution (pH 7.4).[36]

To investigate the ability of ACNT to sensitively detect target molecules, ACNTs were incubated with thrombin molecules at various concentrations (*i.e.* 1 pM–1 nM). We have observed that both tmAFM and KPFM can image the ACNT bound with thrombin molecules at different concentrations (Fig. 4(a) and (b)). This suggests that the SPM technique is able to identify and detect the specific biomolecules with high sensitivity without any labeling process. In particular, the surface coverage of the thrombin bound to the ACNT increases as the thrombin concentration increases, as shown in both the tmAFM and KPFM images. To quantify the biomolecular binding event, we have introduced dimensionless measures – dimensionless height and surface potential defined as $\bar{h} = (h_B - h_0)/h_0$ and $\bar{E} = (E_B - E_0)/E_0$, where h_B and E_B indicate the average height and surface potential, respectively, of an ACNT treated with thrombin, whereas h_0 and E_0 represent the average height and surface potential, respectively, of a bare ACNT. These quantities may be

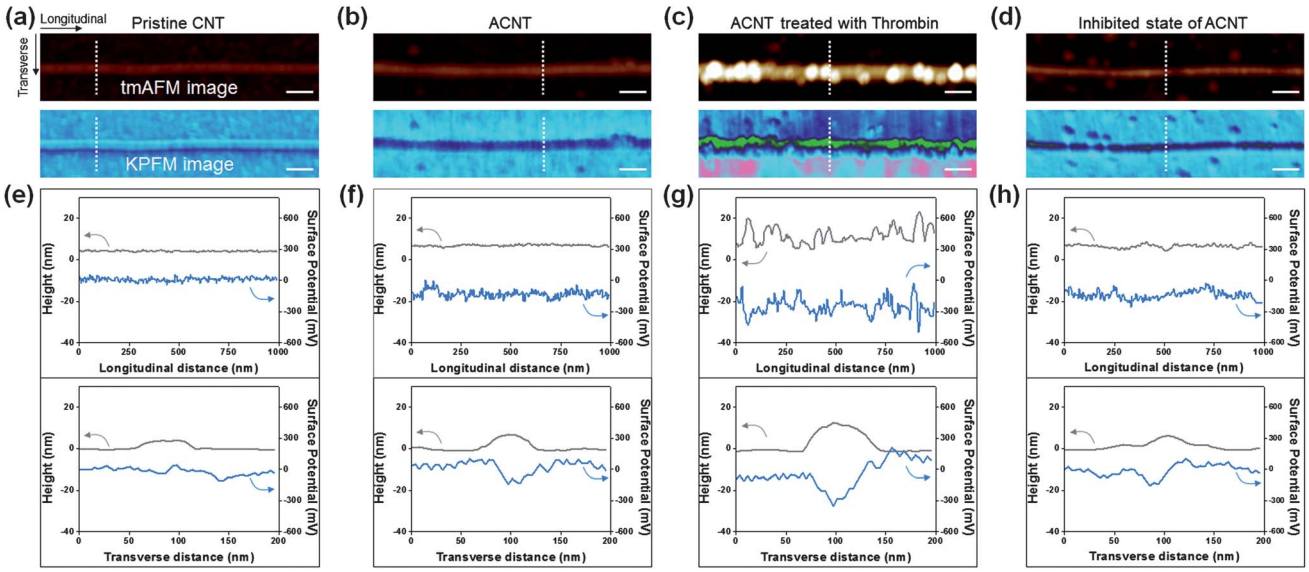

Fig. 3 (a)–(d) tmAFM (upper panel) and KPFM (lower panel) images for pristine CNT, ACNT, ACNT treated with thrombin and for ACNT that are obtained from inhibition assay. (e)–(h) The height and line potential profiles from tmAFM and KPFM images for the height and line potential obtained along the longitudinal (upper graph) and transverse (lower graph) directions. Scale bar is 100 nm.

regarded as the sensing responses to the molecular binding onto ACNT for tmAFM- and KPFM-based detections, respectively. The dimensionless height for thrombin at a concentration of 1 nM is $\sim 1.19 \pm 0.037$ ($n = 3$) while it is given as $\sim 0.002 \pm 0.009$ at a thrombin concentration of 1 pM, which indicates that the dimensionless height enables one to gain a quantitative insight into the sensing response of the ACNT (Fig. 4(c)). As shown in Fig. 4(c), the detection limit for dimensionless height-based sensing is $\sim$10 pM (because a thrombin concentration of 10 pM is close to that at 1 pM), while the detection limit can be improved (even up to 1 pM) using the dimensionless surface potential. This detection sensitivity (*i.e.* $\sim$1 pM) of our method is comparable to that of fluorescence-based detection using signal amplification *via* DNA hybridization,[37] whereas our method does not require any labeling and/or signal amplifications (see selectivity and sensitivity section).

Inhibition bioassay

To verify the robustness of the ACNT as a drug-screening toolkit, we have also considered an inhibition bioassay using an antithrombin. Fig. 3(d) shows the tmAFM/KPFM images for an antithrombin-inhibited ACNT. The magnitudes of both tmAFM height and KPFM surface potential measured in an inhibition assay are significantly reduced in comparison with the binding assay (Fig. 3(d) and (h)). This result supports the antithrombin as being competitively bound to thrombin resulting in the inhibition of thrombin–aptamer binding. Therefore, ACNT can serve as a versatile, robust molecular pattern for studying the drug-induced inhibition mechanism.

To understand the inhibition of thrombin–ACNT binding with respect to antithrombin concentrations, we have implemented tmAFM/KPFM imaging of ACNTs that are exposed to thrombin (100 pM) as well as antithrombin at concentrations ranging from 10 pM to 10 nM. As shown in Fig. 4(d)–(f), as the concentration of antithrombin increases, the number of bright spots corresponding to thrombin molecules bound to ACNT is decreased, in both tmAFM/KPFM images. This confirms the ability of SPM coupled with ACNT to depict the antithrombin-induced inhibition of thrombin–DNA binding. To characterize the antithrombin-driven inhibition of thrombin–DNA binding, we have employed the aforementioned dimensionless height and surface potential, respectively. Fig. 4(f) shows that the dimensionless height enables a quantification of the inhibition mechanism. In particular, the dimensionless height for the inhibition due to antithrombin at a concentration of 10 pM is estimated as $\sim 0.34 \pm 0.010$, while the dimensionless height for an antithrombin concentration of 10 nM is found to be $\sim 0.001 \pm 0.063$. However, the dimensionless height is unable to quantitatively distinguish the inhibition mechanism at an antithrombin concentration of 10^2 pM from that at 10^3 or 10^4 pM, which indicates that tmAFM imaging is incapable of sensitively quantifying the inhibition mechanism at the low concentration of inhibitor molecules. On the other hand, this limitation has been shown to be resolved by KPFM imaging. Specifically, the better detection sensitivity for KPFM than tmAFM is ascribed to the detection principle, that is, KPFM measures the effective charge of biomolecules rather than the change of surface morphology upon biomolecular binding. This suggests that the dimensionless surface potential is a useful measure enabling a sensitive quantification of the inhibition of protein-DNA interactions even at extremely low concentrations of inhibition molecules.

Discussion

Selectivity and sensitivity

For the future application of our fabricated ACNT as a diagnostic tool, we have validated the robustness of our bioassay based on ACNT. First, we have considered whether our ACNT exhibits the capability for selective detection of target protein

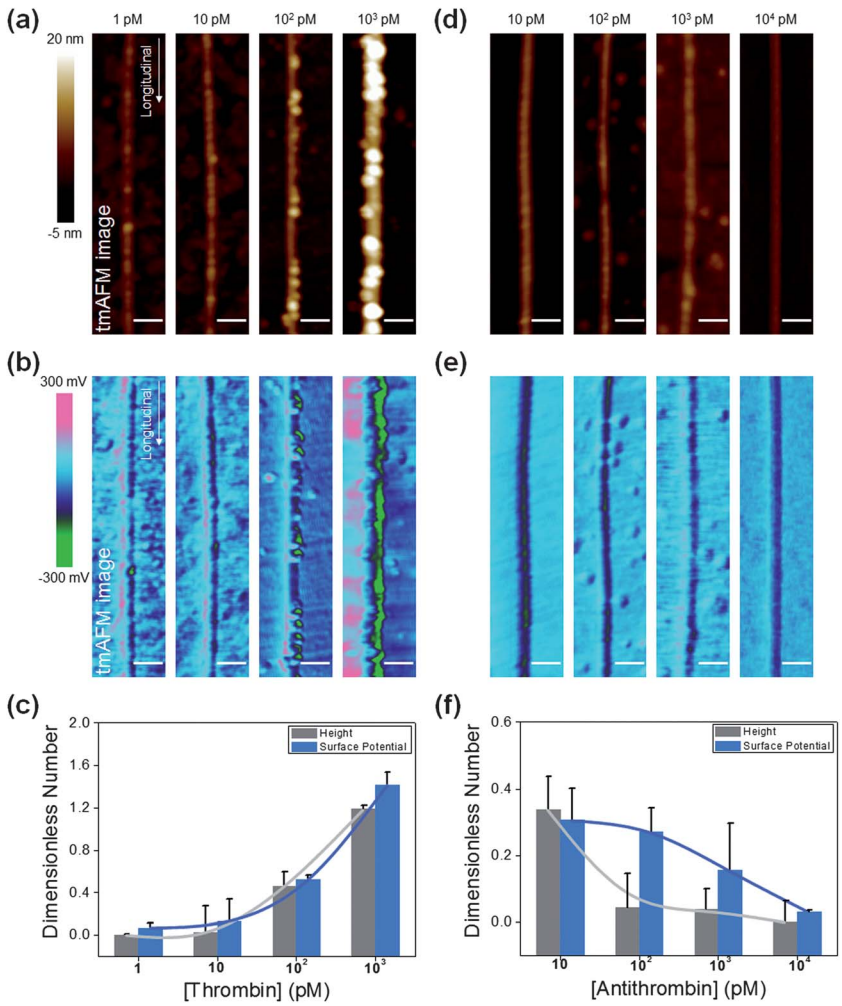

Fig. 4 Quantitative characterization of detection sensitivity for ACNT based on SPM images. (a) tmAFM images and (b) KPFM images of ACNTs that were treated with different thrombin concentrations from 1 pM to 1 nM. (c) Dimensionless height and dimensionless surface potential with respect to thrombin concentration. (d) tmAFM images and (e) KPFM images for ACNTs that are obtained from an inhibition assay at four different concentrations of antithrombin from 10 pM to 10 nM with a fixed thrombin concentration of 100 pM, respectively. Scale bar of all images is 100 nm. (f) Dimensionless height and dimensionless surface potential for ACNT as a function of antithrombin concentrations. Dimensionless quantities were measured based on $n = 3$ (*i.e.* three individual ACNTs).

molecules in a sample that contains different types of biomolecules. Selectivity is a key issue in designing a sensing element that allows for highly sensitive detection, since undesirable physisorption of other biomolecules rather than target biomolecules will lead to a decrease in the reliability of the sensing element due to false positives driven by physisorption, which implies restrictions in early diagnostics. In order to verify the specificity of our ACNT, we have considered a bioassay, in which a sample containing protein molecules (*e.g.* human serum albumin (HSA), fibrinogen, and transferrin) was dropped into our sensing element (*i.e.* ACNT). Fig. 5(a) and (b) show both the AFM images and KPFM images of ACNTs treated with samples containing HSA, transferrin, fibrinogen, and thrombin, respectively (for details of sample treatment, see ESI†). It is shown that the surface morphology and surface potential of the ACNTs have not been changed when treated with samples containing HSA, transferrin, and fibrinogen, respectively, which indicates that the undesirable physisorption of such proteins (rather than thrombin) is unlikely to occur. On the other hand, we have found the surface morphology change and surface potential change for the ACNT when treated with thrombin, which suggests that the ACNT is able to specifically interact with thrombin. In summary, we have shown the ability of the ACNT to selectively capture the target biomolecule (here, thrombin) rather than any other biomolecules.

For future applications in early diagnostics, it is essential to design a sensing element that is able to highly sensitively detect target molecules. In our work, we have shown that our ACNT is able to detect thrombin molecules even at a low concentration (such as 1 pM). The detection sensitivity of our ACNT (*i.e.* 1 pM) is much higher than that of other sensing methods such as surface plasmon resonance (with a sensitivity of 5 nM), electrochemical method (with a sensitivity of 10 pM), impedimetric method (with a sensitivity of 10 nM), and quartz crystal microbalance (with a sensitivity of 0.1 nM). The remarkable detection sensitivity of our sensing method is attributed to the detection principle that we measure the surface morphology and surface potential of thrombin molecules that are specifically bound to the ACNT

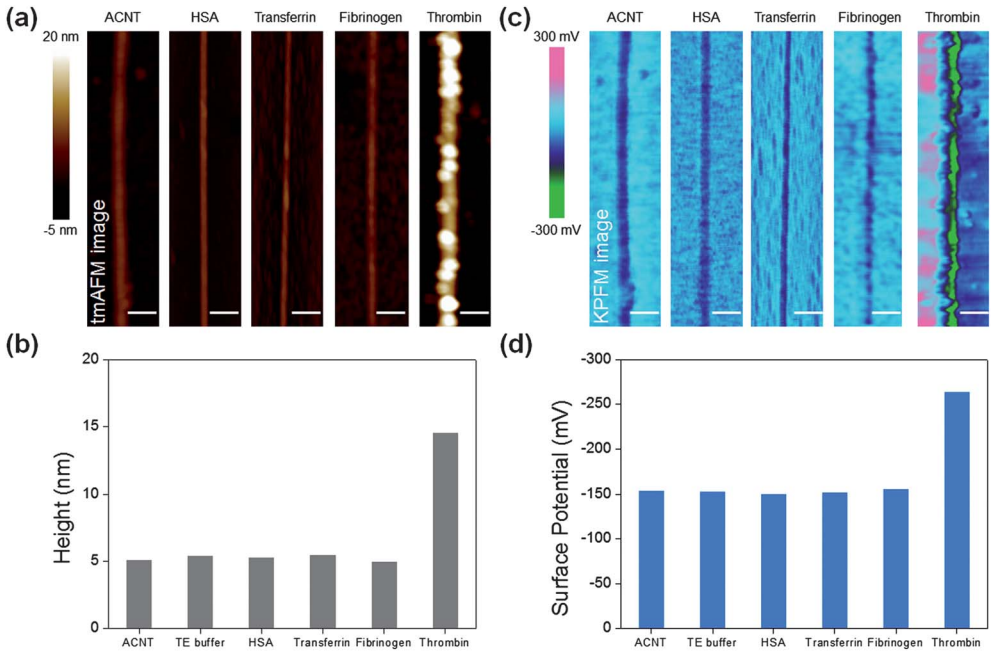

Fig. 5 Selectivity of our ACNT-based bioassay. (a) tmAFM images and (b) KPFM images of ACNTs treated with solutions containing human serum albumin (HSA), transferrin, fibrinogen, and thrombin, respectively. (c) tmAFM heights and (d) surface potentials of ACNTs treated with the aforementioned solutions.

using AFM/KPFM imaging techniques. In particular, the resolution of AFM/KPFM imaging-based detection is in the order of ~10 nm (*e.g.* see Fig. 3 showing that the surface morphology change of ACNT due to thrombin binding is ~15 nm), which is comparable to the size of a single thrombin (*i.e.* the size of thrombin is ~10 nm as reported in ref. 38 and protein data bank with pdb code of 1 ppb). This indicates that our AFM/KPFM imaging-based detection enables the visualization of even minute amounts of thrombin molecules (maybe even up to single-molecule level) specifically bound to an ACNT, which eventually results in the high detection sensitivity of our ACNT-based sensing method using AFM/KPFM imaging techniques.

Effect of solvent condition on protein bioassay

We have studied the effect of solvent conditions on our ACNT-based thrombin detection because solvent conditions (*e.g.* salt concentration, pH, *etc.*) may affect the binding affinity[39] between thrombin and the DNA aptamer functionalized on the CNT. First, we have investigated the role of salt concentration in the binding affinity between thrombin and the ACNT (*i.e.* DNA aptamer functionalized on CNT), since salt concentration makes a critical effect on the Debye screening length of biomolecules, and consequently, the electrostatic interactions between biomolecules, which leads to a change in the binding affinity between biomolecules, as reported in the literature.[40,41] Fig. 6(a) shows the AFM images of ACNT treated with thrombin dissolved in solution with salt concentrations of 0 M, 0.01 M, 0.1 M, and 0.2 M, respectively. It is shown that the number of thrombin molecules bound to the ACNT decreases when the salt concentration increases (see also Fig. 6(b)), which is consistent with previous work[42,43] reporting that an increase in salt concentration reduces the binding affinity between thrombin and a DNA aptamer. This indicates that for future applications of our ACNTs to early diagnosis, it is recommended that salt ions have to be separated from a sample (buffer solution containing biomolecules) before the ACNT-based bioassay is implemented; the separation of ions from buffer solution can be conducted using recently suggested assays such as a nanopore assay[44] and/or micro/nanofluidic assay.[45]

We have also studied the role of the pH of a solvent in the binding affinity between thrombin and ACNT (*i.e.* DNA aptamer functionalized on CNT), since it has been suggested that the pH of a solvent can also make an impact on the binding affinity between biomolecules. Fig. 6(c) provides the AFM images of the ACNT treated with thrombin-dissolved solution whose pH is given as 6, 7, 7.4, and 8, respectively. As shown in Fig. 6(c), the maximum binding affinity between thrombin and the DNA aptamer is at pH 7.4, while the binding affinity decreases when the pH is far from pH 7.4 (see also Fig. 6(d)). This suggests that the detection sensitivity of our ACNT-based bioassay is critically dependent on the pH of a solvent. In other words, when pH is increasing or decreasing from pH 7.4, the detection sensitivity of our bioassay is depreciated. This is consistent with a previous study[42] suggesting that the optimal pH of a solvent for maximum binding affinity between biomolecules is given by pH 7.4.

As described above, the solvent condition (*e.g.* salt concentration, and pH) plays a key role in the detection sensitivity of our ACNT-based bioassay. The optimal condition of a buffer solution for highly sensitive detection is suggested as being a salt concentration of 0 M, and a pH of 7.4. For our future work in which a more realistic sample (*e.g.* blood serum) is used in our bioassay, how to control the salt concentration and pH of a sample has to be taken into account in order to improve the detection sensitivity of our ACNT-based bioassay.

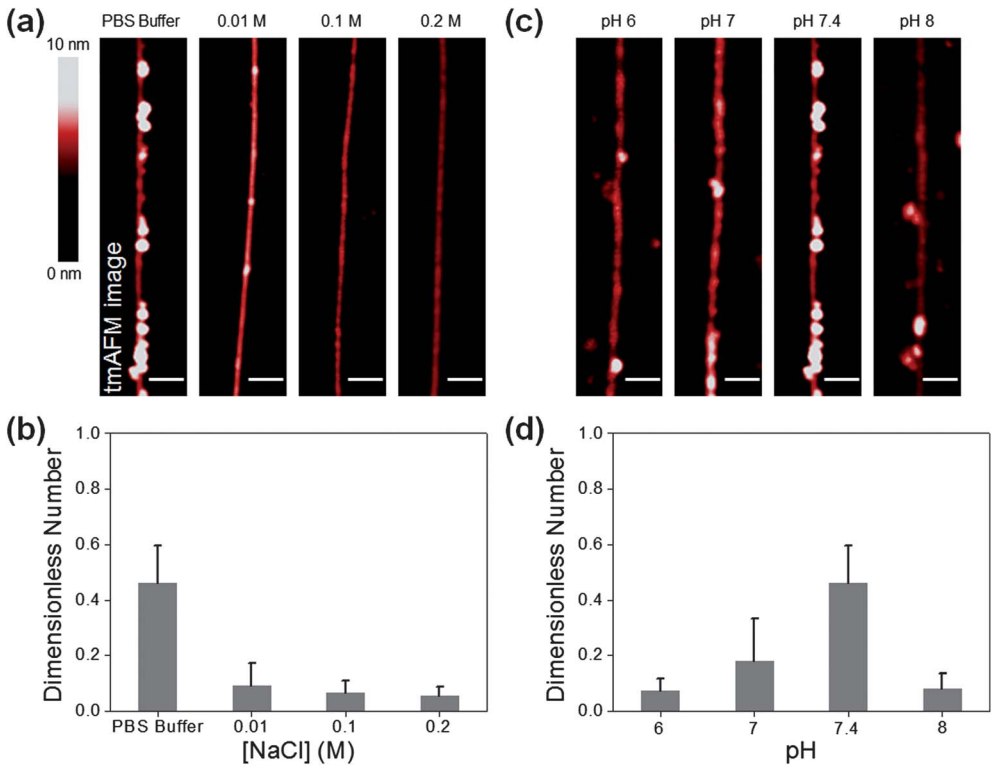

Fig. 6 Quantitative characterization of solvent effects on the binding affinity between thrombin and the ACNT. (a) tmAFM images of ACNTs treated with thrombin dissolved in solutions whose salt concentrations range from 0 M to 0.2 M. (b) Dimensionless height for ACNT treated with aforementioned thrombin solutions as a function of salt concentration of such solution. (c) tmAFM images of ACNTs treated with thrombin solution whose pH is given as 6, 7, 7.4, or 8. (d) Dimensionless height for ACNT treated with thrombin solutions with different pH as a function of the pH of such solution.

Conclusions

In summary, we have developed the ACNT-based label-free biomolecular recognition system coupled to SPM for not only sensitive, selective protein detection but also quantitative characterization of the binding affinity between a biomolecule and the ACNT. Specifically, SPM is able to visualize the molecular recognition using ACNT that can specifically interact with target biomolecules even at concentrations as low as 1 pM. The detection limit of our method is better than that of fluorescence imaging-based detection; to the best of our knowledge, fluorescence imaging-based sensing method exhibits a detection sensitivity of ~1 pM using signal amplifications,[37,46] while our method does not employ any labeling and/or signal amplification to achieve a detection sensitivity of ~1 pM. Moreover, the detection sensitivity of our method is much higher than other label-free sensing methods (see section selectivity and sensitivity). This implies that biomolecular detection using the ACNT *via* an SPM technique is suitable for sensitive diagnostics of specific diseases such as cancer and vascular diseases. Moreover, an ACNT-based biomolecular detection system allows for the quantitative characterization of specific biomolecular interactions and/or inhibitions of such interactions. In particular, our ACNT-based system enables the quantitative characterization of the binding affinity between protein molecules and the ACNT as well as the effect of the chemical environment (*i.e.* pH and ion concentration) on such binding affinity. Our study suggests that our ACNT system would be useful in gaining a quantitative insight into the binding affinity between various biomolecular interactions, which is an *a priori* requisite for the effective design of a sensing element. For future applications in diagnostics and drug screening, our ACNT-based chip could be employed for multiplex sensing[47,48] of biomolecules using more realistic samples such as blood serum (with pretreatment such as dilution).[38,45]

List of abbreviations

ACNT	Aptamer-conjugated carbon nanotube,
CNT	Carbon nanotube,
SPM	Scanning probe microscopy,
tmAFM	Tapping-mode atomic force microscopy,
AFM	Atomic force microscopy,
KPFM	Kelvin probe force microscopy,
CVD	Chemical vapor deposition.

Acknowledgements

This work was supported by the National Research Foundation of Korea (NRF) under Grant No. NRF-2010-0009428, NRF-2011-0009885 and NRF-2010-0027238.

References

1 T. Hermann and D. J. Patel, *Science*, 2000, **287**, 820.
2 D. H. J. Bunka and P. G. Stockley, *Nat. Rev. Microbiol.*, 2006, **4**, 588.
3 G. A. Zelada-Guillén, J. Riu, A. Düzgün and F. X. Rius, *Angew. Chem., Int. Ed.*, 2009, **48**, 7334.
4 E. J. Cho, J.-W. Lee and A. D. Ellington, *Annu. Rev. Anal. Chem.*, 2009, **2**, 241.
5 Y. Xiao, A. A. Lubin, A. J. Heeger and K. W. Plaxco, *Angew. Chem., Int. Ed.*, 2005, **44**, 5456.
6 H. Chang, L. Tang, Y. Wang, J. Jiang and J. Li, *Anal. Chem.*, 2010, **82**, 2341.
7 S. Bi, T. Zhao and B. Luo, *Chem. Commun.*, 2012, **48**, 106.
8 S. D. Jayasena, *Clin. Chem.*, 1999, **45**, 1628.
9 S. Tombelli, M. Minunni and M. Mascini, *Methods*, 2005, **37**, 48.
10 Y. Li, H. J. Lee and R. M. Corn, *Nucleic Acids Res.*, 2006, **34**, 6416.
11 Y. Li, H. J. Lee and R. M. Corn, *Anal. Chem.*, 2007, **79**, 1082.
12 E. E. Ferapontova, E. M. Olsen and K. V. Gothelf, *J. Am. Chem. Soc.*, 2008, **130**, 4256.
13 U. Feldkamp and C. M. Niemeyer, *Angew. Chem., Int. Ed.*, 2006, **45**, 1856.
14 S. H. Park, C. Pistol, S. J. Ahn, J. H. Reif, A. R. Lebeck, C. Dwyer and T. H. LaBean, *Angew. Chem., Int. Ed.*, 2006, **45**, 735.
15 K. Eom, H. S. Park, D. S. Yoon and T. Kwon, *Phys. Rep.*, 2011, **503**, 115.
16 D. Zhou, K. Sinniah, C. Abell and T. Rayment, *Angew. Chem., Int. Ed.*, 2003, **42**, 4934.
17 S. Husale, H. H. J. Persson and O. Sahin, *Nature*, 2009, **462**, 1075.
18 A. K. Sinensky and A. M. Belcher, *Nat. Nanotechnol.*, 2007, **2**, 653.
19 C. Leung, H. Kinns, B. W. Hoogenboom, S. Howorka and P. Mesquida, *Nano Lett.*, 2009, **9**, 2769.
20 P. Gao and Y. Cai, *Anal. Bioanal. Chem.*, 2009, **394**, 207.
21 J. Park, J. Yang, G. Lee, C. Y. Lee, S. Na, S. W. Lee, S. Haam, Y.-M. Huh, D. S. Yoon, K. Eom and T. Kwon, *ACS Nano*, 2011, **5**, 6981.
22 Z. Jin, H. Chu, J. Wang, J. Hong, W. Tan and Y. Li, *Nano Lett.*, 2007, **7**, 2073.
23 B. H. Hong, J. Y. Lee, T. Beetz, Y. Zhu, P. Kim and K. S. Kim, *J. Am. Chem. Soc.*, 2005, **127**, 15336.
24 E. Katz and I. Willner, *ChemPhysChem*, 2004, **5**, 1084.
25 A. Hirsch, *Angew. Chem., Int. Ed.*, 2002, **41**, 1853.
26 J. A. Robinson, E. S. Snow, Ş. C. Bădescu, T. L. Reinecke and F. K. Perkins, *Nano Lett.*, 2006, **6**, 1747.
27 T. J. Simmons, J. Bult, D. P. Hashim, R. J. Linhardt and P. M. Ajayan, *ACS Nano*, 2009, **3**, 865.
28 R. J. Chen, Y. Zhang, D. Wang and H. Dai, *J. Am. Chem. Soc.*, 2001, **123**, 3838.
29 S. Lyonnais, L. Goux-Capes, C. Escudé, D. Cote, A. Filoramo and J.-P. Bourgoin, *Small*, 2008, **4**, 442.
30 J. Yang, K. Eom, E.-K. Lim, J. Park, Y. Kang, D. S. Yoon, S. Na, E. K. Koh, J.-S. Suh, Y.-M. Huh, T. Y. Kwon and S. Haam, *Langmuir*, 2008, **24**, 12112.
31 S. Wang, H. Wang, J. Jiao, K.-J. Chen, G. E. Owens, K.-i. Kamei, J. Sun, D. J. Sherman, C. P. Behrenbruch, H. Wu and H.-R. Tseng, *Angew. Chem., Int. Ed.*, 2009, **48**, 8970.
32 D. Zhou, K. Sinniah, C. Abell and T. Rayment, *Langmuir*, 2002, **18**, 8278.
33 A. Javey, M. Shim and H. Dai, *Appl. Phys. Lett.*, 2002, **80**, 1064.
34 M. Shiraishi and M. Ata, *Carbon*, 2001, **39**, 1913.
35 R. Friedrich, P. Panizzi, P. Fuentes-Prior, K. Richter, I. Verhamme, P. J. Anderson, S.-I. Kawabata, R. Huber, W. Bode and P. E. Bock, *Nature*, 2003, **425**, 535.
36 J. Hu, P.-C. Zheng, J.-H. Jiang, G.-L. Shen, R.-Q. Yu and G.-K. Liu, *Anal. Chem.*, 2009, **81**, 87.
37 Y. Li, Y. T. H. Cu and D. Luo, *Nat. Biotechnol.*, 2005, **23**, 885.
38 W. Bode, I. Mayr, U. Baumann, R. Huber, S. R. Stone and J. Hofsteenge, *EMBO J.*, 1989, **8**, 3467.
39 Z. Zhe, W. Shawn and A. Emil, *Phys. Biol.*, 2011, **8**, 035001.
40 H. H. Strey, V. A. Parsegian and R. Podgornik, *Phys. Rev. E: Stat. Phys., Plasmas, Fluids, Relat. Interdiscip. Top.*, 1999, **59**, 999.
41 H. H. Strey, V. A. Parsegian and R. Podgornik, *Phys. Rev. Lett.*, 1997, **78**, 895.
42 T. Hianik, V. Ostatná, M. Sonlajtnerova and I. Grman, *Bioelectrochemistry*, 2007, **70**, 127.
43 P.-H. Lin, R.-H. Chen, C.-H. Lee, Y. Chang, C.-S. Chen and W.-Y. Chen, *Colloids Surf., B*, 2011, **88**, 552.
44 C. Y. Lee, W. Choi, J.-H. Han and M. S. Strano, *Science*, 2010, **329**, 1320.
45 S. J. Kim, S. H. Ko, K. H. Kang and J. Han, *Nat. Nanotechnol.*, 2010, **5**, 297.
46 S. Niu, L. Qu, Q. Zhang and J. Lin, *Anal. Biochem.*, 2012, **421**, 362.
47 S. I. Stoeva, J.-S. Lee, C. S. Thaxton and C. A. Mirkin, *Angew. Chem., Int. Ed.*, 2006, **45**, 3303.
48 F. Patolsky, G. Zheng and C. M. Lieber, *Anal. Chem.*, 2006, **78**, 4260.